

PAPER

## Atomic layer deposited high- $k$ dielectric on graphene by functionalization through atmospheric plasma treatment

To cite this article: Jeong Woo Shin *et al* 2018 *Nanotechnology* **29** 195602

View the [article online](#) for updates and enhancements.



**IOP | ebooks™**

Bringing you innovative digital publishing with leading voices to create your essential collection of books in STEM research.

Start exploring the collection - download the first chapter of every title for free.

# Atomic layer deposited high-*k* dielectric on graphene by functionalization through atmospheric plasma treatment

Jeong Woo Shin<sup>1,3</sup>, Myung Hoon Kang<sup>2,3</sup>, Seongkook Oh<sup>1</sup>,  
Byung Chan Yang<sup>1</sup>, Kwonil Seong<sup>1</sup>, Hyo-Sok Ahn<sup>1</sup>, Tae Hoon Lee<sup>2,4</sup>  and  
Jihwan An<sup>1,4</sup> 

<sup>1</sup> Department of Manufacturing Systems and Design Engineering (MSDE), Seoul National University of Science and Technology (SeoulTech), Seoul 01811, Republic of Korea

<sup>2</sup> Department of Electrical Engineering, Kwangwoon University, Seoul 01897, Republic of Korea

E-mail: [lthoon@kw.ac.kr](mailto:lthoon@kw.ac.kr) and [jihwanan@seoultech.ac.kr](mailto:jihwanan@seoultech.ac.kr)

Received 10 November 2017, revised 9 February 2018

Accepted for publication 20 February 2018

Published 13 March 2018



CrossMark

## Abstract

Atomic layer-deposited (ALD) dielectric films on graphene usually show noncontinuous and rough morphology owing to the inert surface of graphene. Here, we demonstrate the deposition of thin and uniform ALD ZrO<sub>2</sub> films with no seed layer on chemical vapor-deposited graphene functionalized by atmospheric oxygen plasma treatment. Transmission electron microscopy showed that the ALD ZrO<sub>2</sub> films were highly crystalline, despite a low ALD temperature of 150 °C. The ALD ZrO<sub>2</sub> film served as an effective passivation layer for graphene, which was shown by negative shifts in the Dirac voltage and the enhanced air stability of graphene field-effect transistors after ALD of ZrO<sub>2</sub>. The ALD ZrO<sub>2</sub> film on the functionalized graphene may find use in flexible graphene electronics and biosensors owing to its low process temperature and its capacity to improve device performance and stability.

Supplementary material for this article is available [online](#)

Keywords: atmospheric plasma, atomic layer deposition, graphene, graphene field effect transistor, high-*k* dielectric

(Some figures may appear in colour only in the online journal)

## Introduction

Graphene has been extensively studied as a promising candidate material for flexible electronics [1, 2] and wearable biosensors [3] owing to its outstanding mechanical flexibility [4], high carrier mobility [5], high surface-to-volume ratio [6], and biocompatibility [7]. In particular, sensors based on graphene field-effect transistors (GFETs) have high sensitivity owing to the high transconductance of GFETs [8]. For achieving GFET sensors of high sensitivity and stability, the deposition of thin and uniform high-*k* dielectric films on graphene is of great importance. In graphene biosensors, for

instance, the direct surface modification of graphene with linkers or receptors causes a disordered potential in graphene which decreases the charge transport and sensitivity of GFET sensors [9, 10]. Thin and high-*k* dielectric films between graphene and receptors suppress the disordered potential induced from linkers or receptors [9] and help to enhance the sensitivity of GFET biosensors by increasing the field-effect from target analytes [11]. An additional role of uniform (pin-hole free and continuous) dielectric films is passivation of graphene to prevent performance instability of GFETs owing to environmental sources such as H<sub>2</sub>O/O<sub>2</sub> in air and biological materials in body fluids [12, 13].

Among various deposition methods for a dielectric layer, atomic layer deposition (ALD) is advantageous for depositing ultra-thin uniform films [14, 15]. ALD is a modified form of

<sup>3</sup> These authors contributed equally to this work.

<sup>4</sup> Authors to whom any correspondence should be addressed.

chemical vapor deposition (CVD), which can deposit a thin film in an atomic layer-by-layer manner. Owing to its surface-limited reaction mechanism, one can deposit dense and conformal high-quality thin films at relatively low temperatures ( $<300\text{ }^{\circ}\text{C}$ ) [14, 15]. However, ALD relies on the chemisorption or rapid reaction of precursor molecules with the surface functional groups [14]. The inertness of the graphene basal plane due to strong  $\text{sp}^2$  carbon bonding prevents the facile nucleation of dielectric materials on the graphene surface during the ALD process. Thus, various methods for functionalization of the graphene surface have been suggested such as wet chemical treatment, thermal oxidation treatment, and vacuum plasma treatment [16–18]. These techniques functionalize the graphene surface but also often damage or etch away part of the graphene because of the high-energy species that exist during the process [16, 17]. To avoid the etching problem of vacuum plasma treatment, delicate control of plasma power and exposure time has been carried out [17] or samples were placed upside down for indirect exposure to high-energy ions [18]. However, these additional measures may limit the applicability and scalability of vacuum plasma process. Here, we propose an atmospheric plasma treatment for graphene functionalization with minimal structural and electrical degradation. Compared to vacuum plasma, atmospheric plasma has more low-energy radicals and fewer high-energy ions, which makes surface functionalization with low-energy radicals dominant and thus reduces damage to the graphene by bombardment of high-energy ions [19]. Additionally, an atmospheric plasma system is easy to scale up and inexpensive compared to a vacuum plasma system [16].

In this work, we demonstrate that dense and uniform high- $k$  dielectric films of  $\text{ZrO}_2$  can be deposited on graphene using ALD after graphene functionalization through atmospheric plasma treatment. Atomic force microscopy (AFM), scanning electron microscopy (SEM), x-ray diffraction (XRD), x-ray reflectivity (XRR), and transmission electron microscopy (TEM) showed that ALD  $\text{ZrO}_2$  films on the plasma-treated graphene were thin, uniform, and polycrystalline. Electrical characterization revealed that the atmospheric plasma treatment generated functional groups in graphene, shifting the Dirac voltage ( $V_{\text{dirac}}$ ) of the GFETs to positive voltage, and that the ALD of  $\text{ZrO}_2$  on the plasma-treated graphene reduced the number of charge-trapping sites in and around the graphene, recovering the charge transport and  $V_{\text{dirac}}$  ( $\sim 0\text{ V}$ ) in the GFETs. The reduction of charge-trapping sites by the ALD  $\text{ZrO}_2$  films improved the graphene device performance and stability. Consequently, we believe that a combination of atmospheric plasma treatment and ALD may become an important approach to forming thin and uniform dielectric layers on graphene for a variety of graphene-based electronics and sensors.

## Experimental

### *Atmospheric plasma treatment*

Multilayer CVD graphene samples on  $285\text{ nm SiO}_2/\text{Si}$  (highly p-doped) were purchased from Graphene Supermarket. The

detailed growth and transfer methods are described in the literature [20, 21]. According to the AFM analysis, the thickness of the graphene was in the  $2\text{--}20\text{ nm}$  range (figure S1 is available online at [stacks.iop.org/NANO/29/195602/mmedia](http://stacks.iop.org/NANO/29/195602/mmedia)). The plasma was composed of a mixture of argon carrier gas and active gas (oxygen). The plasma conditions were fixed at a radio-frequency ( $13.56\text{ MHz}$ ) power of  $100\text{ W}$ , an oxygen flow rate of  $40\text{ sccm}$ , an argon flow rate of  $8\text{ sccm}$ , and a working distance of  $2\text{ mm}$ . The graphene samples were treated for 3, 10, and 30 passes using a lateral rate of  $25\text{ mm s}^{-1}$ , which correspond to durations of 0.8, 2.4, and 8 s, respectively.

### *ALD of $\text{ZrO}_2$ films*

The  $\text{ZrO}_2$  film was deposited on the surface of the plasma-treated graphene using a home-made ALD station. The ALD of  $\text{ZrO}_2$  was performed using tetrakis(ethylmethylamido)zirconium (TEMA-Zr) and  $\text{H}_2\text{O}$  as a precursor and oxygen source, respectively. TEMA-Zr was heated to  $75\text{ }^{\circ}\text{C}$  and the  $\text{H}_2\text{O}$  was kept at room temperature. Nitrogen gas was used as a carrier gas with a flow rate of  $20\text{ sccm}$  and the chamber was kept at  $150\text{ }^{\circ}\text{C}$ . Each ALD cycle consisted of 4 steps: (1) a  $0.3\text{ s}$  pulse of TEMA-Zr; (2)  $30\text{ s}$  purge; (3)  $0.1\text{ s}$  pulse of  $\text{H}_2\text{O}$ ; and (4)  $30\text{ s}$  purge. The  $\text{ZrO}_2$  film was deposited with 100 cycles.

### *Device fabrication procedure*

The whole device fabrication procedure is shown in the schematic of figure S6. For source/drain contacts,  $150\text{ nm}$ -thick dense platinum electrodes ( $W = 1\text{ mm}$ ,  $L = 1\text{ mm}$ ) were dc-sputtered at a pressure of  $1\text{ Pa}$  in Ar atmosphere with  $400\text{ W}$  power. For graphene functionalization, atmospheric oxygen plasma treatment was conducted for various numbers of plasma passes. Then,  $\text{ZrO}_2$  films were deposited on the functionalized graphene using ALD and source/drain platinum contacts were sputtered onto the  $\text{ZrO}_2$  films, thus fabricating  $\text{ZrO}_2/\text{Pt}/\text{graphene}$ -structured devices.

### *Structural and electrical characterization*

Raman spectroscopy was used to characterize the properties of the plasma-treated graphene. The Raman spectra were measured using a Renishaw and a  $532\text{ nm}$  laser. The graphene was scanned in circular areas  $2\text{ }\mu\text{m}$  in diameter across the surface. Water contact-angle measurements were made on several drops ( $10\text{ }\mu\text{l}$  drops of de-ionized water) placed at three different locations on the surface (KSV, CAM-200). X-ray photoelectron spectroscopy (XPS) was used for compositional analysis [PHI 5000 VersaProbe (Ulvac-PHI)] with an Al  $\text{K}\alpha$  source gun ( $1486.6\text{ eV}$ ), a spot size of  $100\text{ }\mu\text{m} \times 100\text{ }\mu\text{m}$ , a step size of  $0.1\text{ eV step}^{-1}$ , and a binding energy range of  $280\text{--}292\text{ eV}$ . The  $\text{ZrO}_2$  film surface was characterized using a field-emission scanning electron microscope (JSM-6700F, JEOL Ltd). The crystal structure of the ALD  $\text{ZrO}_2$  films was characterized by field-emission TEM (Tecnai F30) operated at  $300\text{ kV}$  with selective area electron diffraction patterns ( $\sim 200 \times 200\text{ nm}$  area). AFM (SmartSPM-1000, AIST-NT) was used to characterize the

surface morphology of the ALD ZrO<sub>2</sub> films. Grazing-incidence x-ray diffraction (GIXRD) and XRR (D8 Discover, Bruker) was used to characterize the crystallinity, thickness, density, and roughness of the ALD ZrO<sub>2</sub> films. The transfer characteristics of the GFETs were measured in air using a Keithley 4200 SCS instrument. The gate voltage was swept from -120 to 120 V, and the drain-source voltage was 1.5 V.

## Results and discussion

Raman spectroscopy of the graphene samples showed the nature of defects on the graphene surfaces treated with different numbers of plasma passes (figures 1(a) and (b)). The G peak (1597 cm<sup>-1</sup>) is known to be produced by the C-C bond of the graphite materials, and the D peak (1350 cm<sup>-1</sup>) is associated with defects on graphene, which causes disorders in the sp<sup>2</sup> bonding of the graphene surface, such as sp<sup>3</sup>-type (dangling bonds), vacancy-type, or boundary-like defects [22]. The fact that the G peak was more intense than the 2D peak in all spectra confirmed that the spectra were obtained from multilayer graphene regions [23]. The D peak was difficult to observe in the untreated graphene, but it increased noticeably as the graphene was functionalized by plasma treatment, as shown in figures 1(b) and S2. Furthermore, specific types of defects, i.e., dangling bonds, vacancies, and boundaries, led to different ratios between the D peak and D' peak (near 1620 cm<sup>-1</sup>) that occurred through an intra-valley double resonance process in the presence of defects [24]. The high relative integrated intensity of the D to D' peak ( $I_D/I_{D'} \approx 13$ ) for the plasma-treated graphene implies that the D peak was mostly a result of dangling bond-type defects rather than vacancy-type ( $I_D/I_{D'} \approx 7$ ) or boundary-type ( $I_D/I_{D'} \approx 3.5$ ) defects (figure 1(c)) [22].

The water contact-angle results measured as the number of plasma passes increased also indicated that the formation of dangling bonds through plasma treatment increased the surface energy, resulting in reduced contact angles (figure 1(d)) [17]. The water contact angle of untreated graphene is 95(±5)°, indicating that the graphene surface is hydrophobic. However, the graphene surface became hydrophilic with water contact angles of 24(±5)°, 10(±5)°, and 6(±5)° after 3, 10, and 30 plasma passes, respectively. This is consistent with the Raman spectroscopy results. Considering the insignificant morphology variation between untreated and treated graphene, we believe that the surface energy increased primarily owing to the formation of dangling bond-type defects, i.e., O-containing groups, after plasma treatment [16]. Previous studies regarding XPS analysis of oxygen plasma-treated graphene surfaces revealed that O-containing groups formed on the graphene surface upon exposure to oxygen plasma may include alkoxy groups (C-O), carbonyl groups (C=O), carboxyl groups (O-C=O), and so on [25]. Indeed, in the XPS analysis of the untreated and the plasma-treated graphene surfaces, a single C-C peak is shown at 284.7 eV in the untreated graphene (figure 1(e)). In contrast, a strong C-O peak (286.9 eV), as well as a relatively weak O-C=O [i.e., C(O)O] peak (288.8 eV), were clearly observed in the plasma-treated graphene (figure 1(f)), which implies the

transformation of sp<sup>2</sup> hybridization to sp<sup>3</sup> hybridization [26]. O-containing groups can easily further react with water vapor in air forming hydroxyl groups (C-O-H), which are preconditions for the subsequent ALD process. The oxygen incorporation ratio, i.e., O/C ratio, on graphene surfaces upon atmospheric O<sub>2</sub> plasma treatment is known to be as high as ~0.1 after only a few passes [16].

The micromorphology and crystallinity of ALD ZrO<sub>2</sub> films (100 cycles) on untreated and plasma-treated graphene are compared in SEM, XRR, XRD, and AFM characterizations (figures 2, S3 and S4). SEM images (figures 2(a) and (b)) show that the untreated graphene is covered with relatively coarse grains with pores while the plasma-treated (10 plasma passes) graphene is covered with fine grains forming a dense layer. The XRR spectra of the ALD ZrO<sub>2</sub> film on the untreated graphene did not show clear indication of film formation, whereas that on the plasma-treated graphene (10 passes) revealed the density (4.34 g cm<sup>-3</sup>), roughness (0.64 nm), and thickness (11.1 nm) of the film (figure 2(c)). It is notable that the ALD ZrO<sub>2</sub> film on the plasma-treated graphene was less dense and its roughness was greater than that on a smooth Si wafer (density: 5.89 g cm<sup>-3</sup>, roughness: ~1% of film thickness) reported elsewhere [27]. In spite of the much-improved uniformity and smoothness of the ZrO<sub>2</sub> film on the plasma-treated graphene as compared to that on the untreated graphene (figures 2(a) and (b)), the fact that the ZrO<sub>2</sub> film on the plasma-treated graphene was less dense and had a rougher microstructure than that on a Si wafer may have contributed to its relatively high leakage current, as will be presented in the following paragraphs. In the GIXRD analysis, the spectra of the ALD ZrO<sub>2</sub> film on the plasma-treated graphene showed a sharp crystalline peak at 29.40° from tetragonal ZrO<sub>2</sub> phase, whereas that on the untreated graphene showed a characteristic amorphous phase (from the standard ICDD, PDF data for the 42-1164 (tetragonal ZrO<sub>2</sub>)) (figure 2(d)). The AFM results further confirmed the morphological differences (figures 2(e)-(g) and S3): the surface roughness of the ALD ZrO<sub>2</sub> films on the plasma-treated graphene for 3, 10, and 30 plasma passes was significantly smaller than that of the untreated graphene [ $R_{\text{rms}}$ : 0.9–1.2 nm (treated) versus 2.6 nm (untreated)]. Figure S3(f) further shows that the grain size clearly decreased as the number of plasma passes increased. The grain size deviation also decreased as the number of plasma passes increased, which implies that the nucleation of the ZrO<sub>2</sub> film occurred simultaneously at the beginning of the deposition process. We think this is due to the O-containing dangling bonds on the graphene surface produced by the oxygen plasma treatment, which led to the formation of a high density of surface O-H dangling bonds by the reaction with moisture in the air. Because the O-H dangling bonds on the surface became nucleation sites for the subsequent ZrO<sub>2</sub> film deposition process, this suggests that the initial nucleation density of the deposition on the plasma-treated graphene surface increased. Thus, dense ZrO<sub>2</sub> films with smaller grains and without pores were deposited. The deposition of the ZrO<sub>2</sub> films on the untreated graphene was mainly due to defects in the

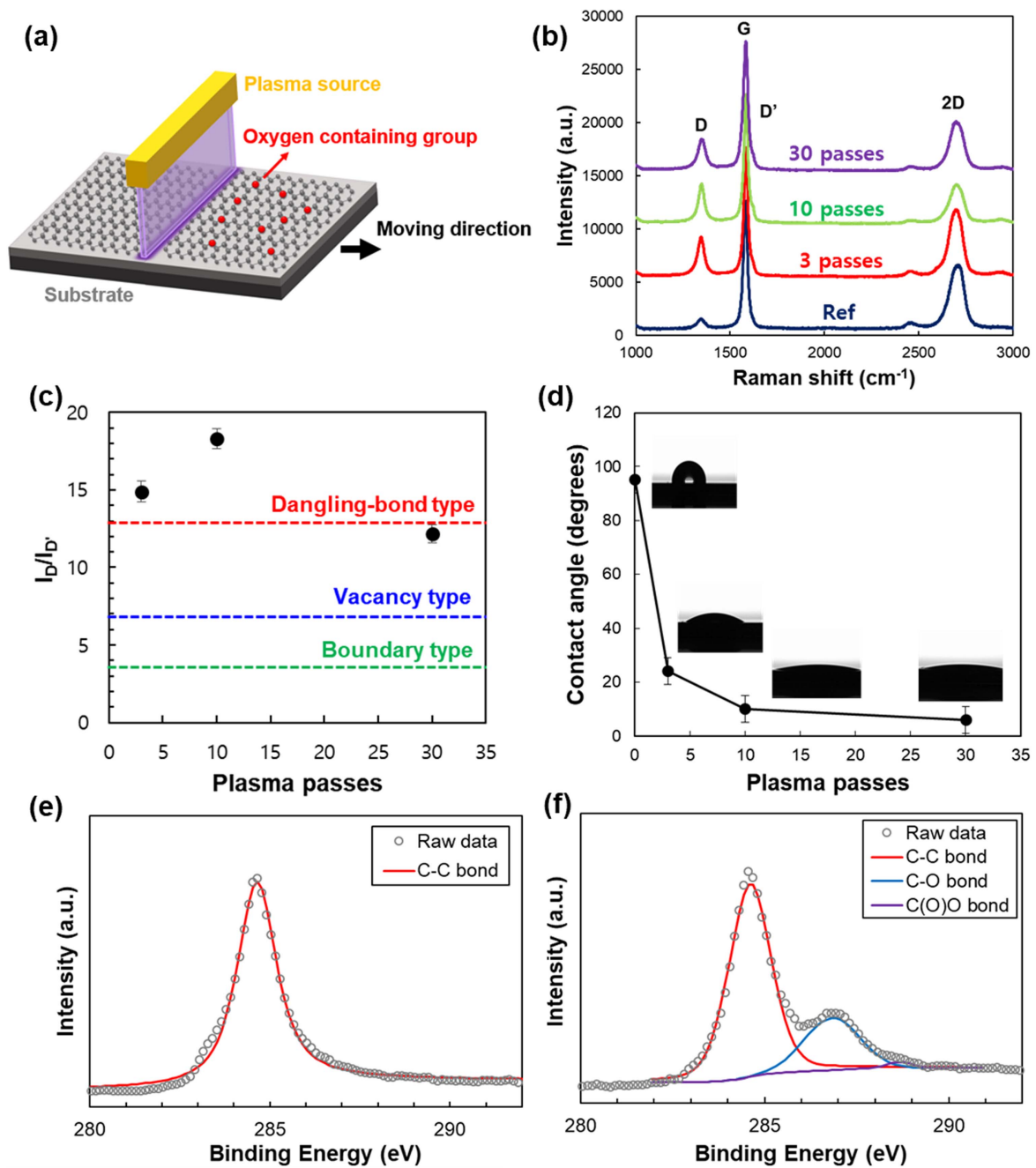


**Figure 1.** (a) Schematic of the atmospheric plasma treatment process, (b) Raman spectra of the untreated (reference) and plasma-treated graphene (3, 10, and 30 passes), (c) relative integrated intensity of the D to D' peak (from the Raman spectra) corresponding to the main type of defects [19], and (d) contact-angle measurement results of the untreated and plasma-treated graphene. XPS spectra of (e) the untreated and (f) the plasma-treated graphene (10 passes).

CVD-grown graphene and/or polymer residues generated in the transfer process.

The TEM images showed pinholes in the  $\text{ZrO}_2$  film deposited on the untreated graphene, as was also seen in the SEM images (figure 3(a)). As the number of plasma passes increased, the  $\text{ZrO}_2$  film became denser, and at three or more plasma passes, it covered the graphene surface almost perfectly (figures 3(b) and S4). A diffraction ring for  $\text{ZrO}_2$  deposited at  $150^\circ\text{C}$  on the untreated graphene was either not present or mostly diffused, which implies that the amorphous phase was dominant (figure 3(c)) [28]. However, for the ALD

$\text{ZrO}_2$  on the plasma-treated graphene, a diffraction ring for tetragonal phase  $\text{ZrO}_2$  was clearly observed (figure 3(d)). The high-resolution TEM images showed the better crystallinity of the ALD  $\text{ZrO}_2$  films on the plasma-treated graphene as compared to that on the untreated graphene (figures 3(e)–(i)), which is in line with the GIXRD results. On the untreated graphene, most of the ALD  $\text{ZrO}_2$  film was amorphous, and only a small portion was crystalline (figures 3(e) and (g)). In contrast, the TEM image of the ALD  $\text{ZrO}_2$  film on the plasma-treated graphene (figure 3(f)) clearly revealed that crystallization was facilitated on the plasma-treated

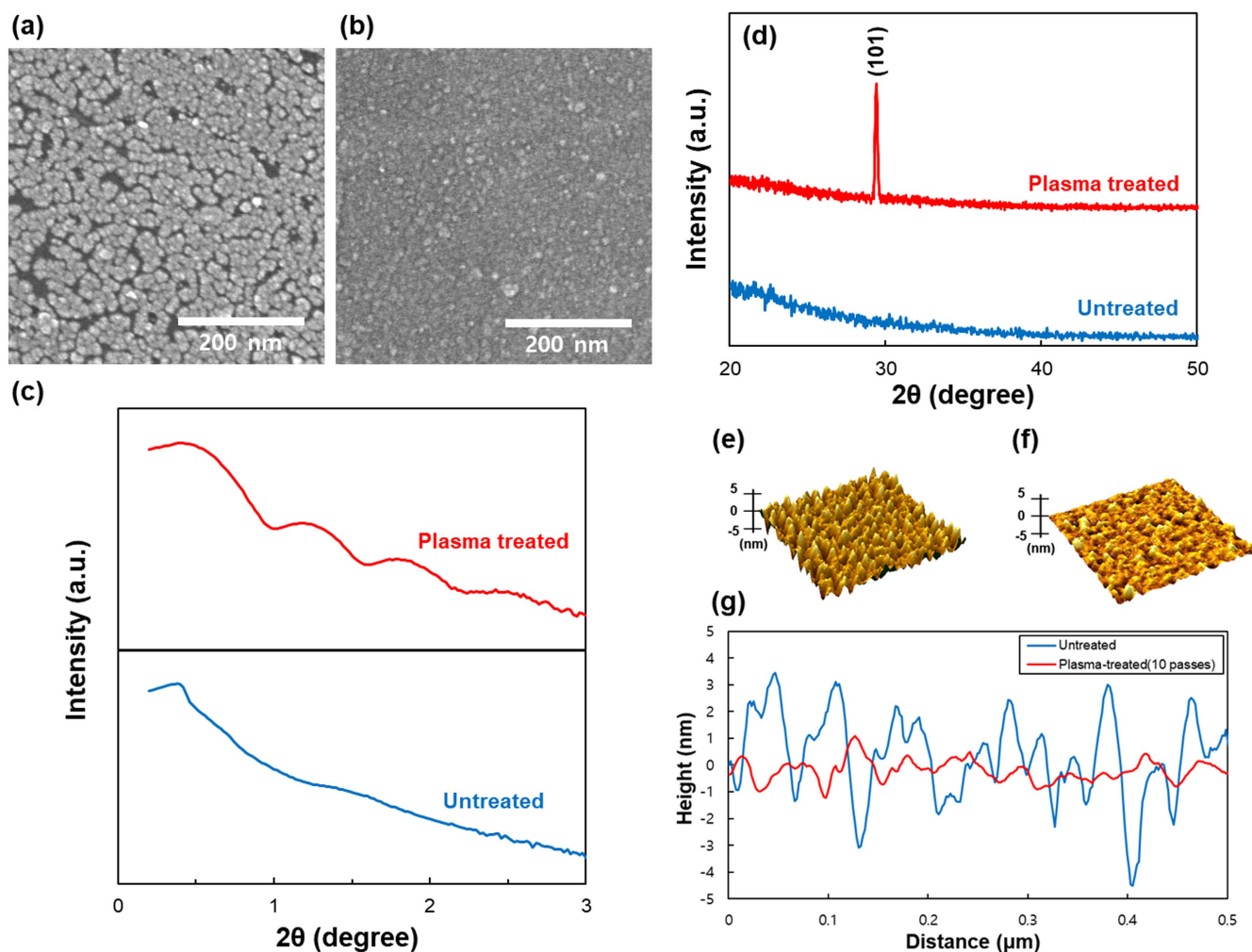


**Figure 2.** SEM images of ALD ZrO<sub>2</sub> films on (a) untreated and (b) plasma-treated graphene (10 passes). Bright regions and dark regions in (a) represent ZrO<sub>2</sub> grains and pores (underlying graphene is shown), respectively. (c) XRR spectra and (d) GIXRD spectra of untreated and plasma-treated graphene (10 passes). AFM topography images (analyzing area: 500 nm × 500 nm) of ALD ZrO<sub>2</sub> films on (e) untreated and (f) plasma-treated graphene (10 passes), and (g) height profile analysis (line length: 500 nm) of the AFM images of ALD ZrO<sub>2</sub> films on untreated and plasma-treated graphene (10 passes).

graphene. A tetragonal ZrO<sub>2</sub> structure with  $a = 0.516 \pm 0.001$  nm and  $c = 0.522 \pm 0.001$  nm ( $a/c$  ratio of 0.986) was observed, as shown in figure 3(i), where the  $\langle 110 \rangle$  zone-axis is perfectly aligned with the electron beam. These values match the crystallographic data for tetragonal ALD ZrO<sub>2</sub> in a previous publication [ $a = 0.510$ – $0.519$  nm,  $c = 0.517$ – $0.522$  nm ( $a/c$  ratio of 0.986–0.988)] [29].

It is notable that the plasma treatment affected not only the areal coverage but also the crystallinity of the ALD ZrO<sub>2</sub> film. It is known that the density and crystallinity of ALD films increase with increasing deposition temperature because thermal energy enhances the surface mobility of adsorbed species, e.g., Zr and/or O ions, and therefore it promotes the ordering of the species that leads to crystallite growth [30]. Indeed, ALD ZrO<sub>2</sub> films (thickness >30 nm) deposited on Si at low temperatures (180 °C and below) have been reported to be amorphous, whereas ALD ZrO<sub>2</sub> films start to crystallize in a tetragonal phase at a high temperature of 300 °C [29]. Liu *et al* reported that they observed the improved crystallinity of ALD ZrO<sub>2</sub> films formed on a graphene nanosheets at a high

temperature of 250 °C, whereas ALD ZrO<sub>2</sub> films deposited at 150 °C were mostly amorphous [30]. However, the high deposition temperature, in turn, often poses a challenge in terms of obtaining uniform films; a high-temperature process causes dihydroxylation of the graphene surface, i.e.,  $2||\text{-OH} \rightarrow ||\text{=O} + \text{H}_2\text{O}$  [30], which may result in the reduction of nucleation sites for ALD. Interestingly, at a low ALD temperature of 150 °C in our experiment, we obtained a thin (~10 nm), uniform, and highly crystalline ALD ZrO<sub>2</sub> film on the plasma-treated graphene, as shown in figure 3(f). We believe this can be attributed to the improved surface mobility of surface intermediates owing to their weak non-covalent interaction with graphene [31, 32]. Such non-covalent interactions have been reported to induce two-dimensional and even epitaxial growth of various materials on graphene [33]. Using such low-temperature ALD to deposit dense and crystalline ZrO<sub>2</sub> films on graphene can have potential benefits for the dielectric performance of the film because the dielectric constant ( $k$ ) of amorphous ZrO<sub>2</sub> is ~20, whereas that of tetragonal ZrO<sub>2</sub> is ~35–50 [34], which may help

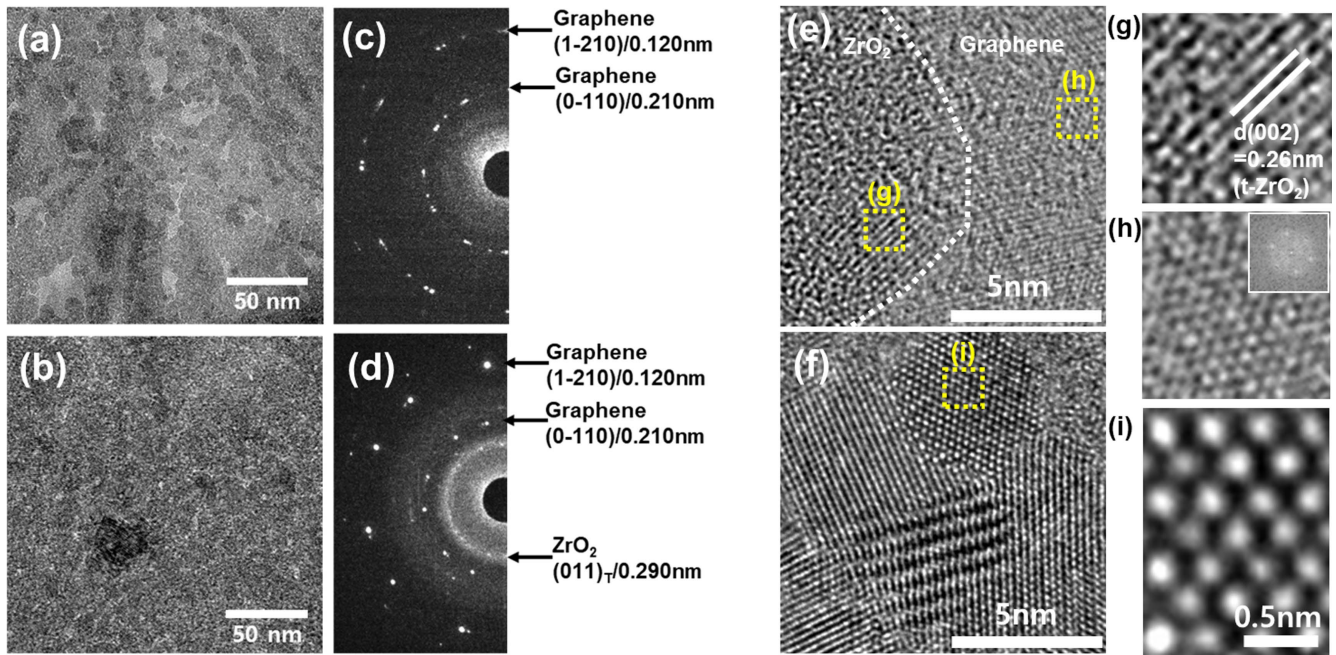


**Figure 3.** TEM images of ALD ZrO<sub>2</sub> films on (a) untreated and (b) plasma-treated graphene (10 passes), with (c), (d) corresponding SAED patterns. High-resolution TEM images of ALD ZrO<sub>2</sub> films on (e) untreated and (f) plasma-treated graphene (3 passes), with zoomed-in images of (g) ZrO<sub>2</sub> particles on untreated graphene, (h) untreated graphene alone, and (i) ZrO<sub>2</sub> particles on plasma-treated graphene, where the bright spots correspond to cation (Zr ion) lattice sites in the tetragonal crystal structure.

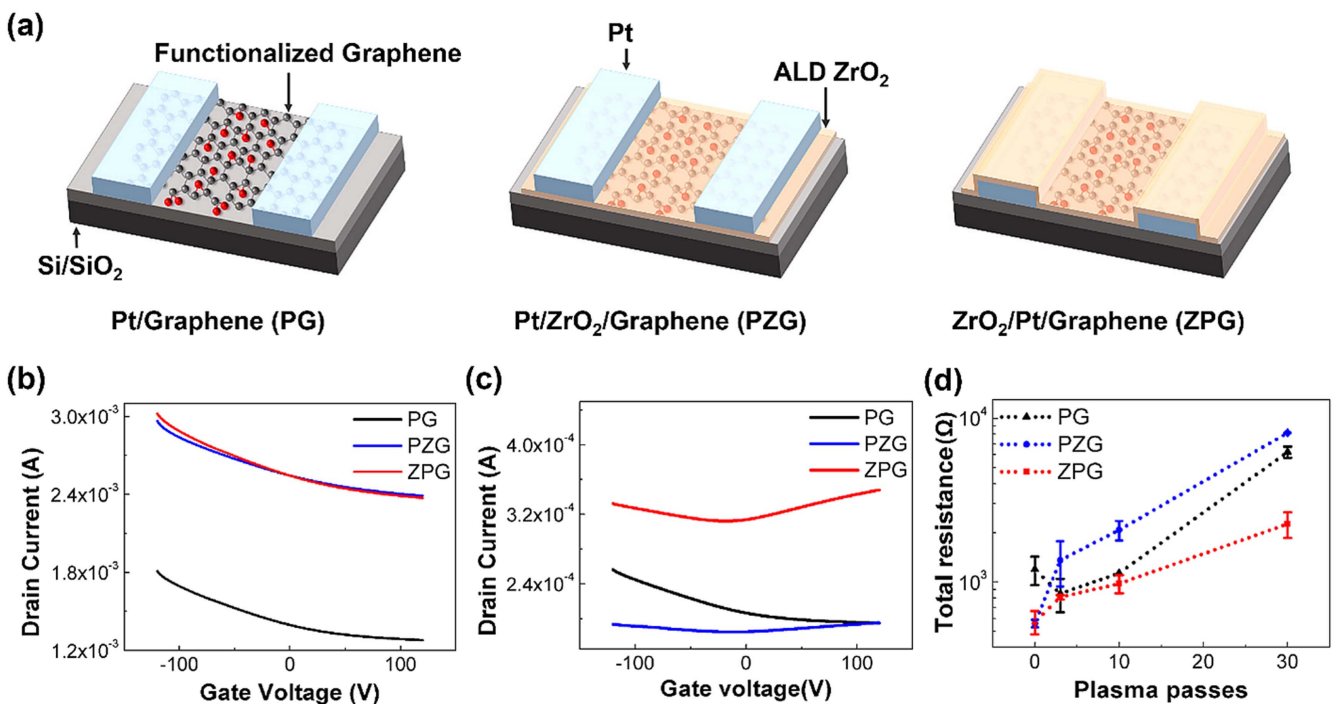


**Figure 4.** (a) Device schematics for Pt/graphene (PG)-, Pt/ZrO<sub>2</sub>/graphene (PZG)-, and ZrO<sub>2</sub>/Pt/graphene (ZPG)-structured GFETs. Transfer characteristics of PG-, PZG-, and ZPG-structured devices with atmospheric plasma treatment for (b) 0 passes and (c) 30 passes (gate voltage range: -120 to 120 V, drain-source voltage: 1.5 V). (d) Total resistance of graphene FETs measured at the floating gate and the drain-source voltage of 1.5 V.

enhance the capacitance and, accordingly, the sensitivity of GFET-based biosensors.

GFETs with three different structures were fabricated and characterized to study the electrical effects of atmospheric plasma treatment and ALD of ZrO<sub>2</sub> on graphene, as shown in

figure 4. The electrical characterization of Pt/graphene (PG)-structured devices after various numbers of plasma passes revealed the effects of the plasma treatment on graphene. The FETs with untreated graphene did not show  $V_{\text{dirac}}$  within the measured gate voltage range of -120 to 120 V (figure 4(b)).

The extremely high  $V_{\text{dirac}}$  is mainly attributed to p-doping by ambient  $\text{H}_2\text{O}/\text{O}_2$  redox couples [12, 35], O-containing groups [36], polymer residues [37], and an interface dipole layer between graphene and platinum electrodes [38]. The ALD of  $\text{ZrO}_2$  did not significantly change the high  $V_{\text{dirac}}$  of the FETs with untreated graphene (figure 4(b)). Because the ALD  $\text{ZrO}_2$  films on untreated graphene were noncontinuous with many pinholes because of the lack of nucleation sites on the untreated graphene surface (figure 2(a)), they did not fully passivate graphene from ambient  $\text{H}_2\text{O}$  and  $\text{O}_2$ , which accounts for the high  $V_{\text{dirac}}$  of the GFETs, even after ALD of  $\text{ZrO}_2$ .

However, the ALD  $\text{ZrO}_2$  films on plasma-treated graphene played an important role as passivation layers for graphene (figure 4(c)). The O-containing groups generated by plasma treatment such as epoxide and hydroxyl groups have an electronegative character that lowers the Fermi energy level of graphene [36]. Thus, plasma treatment further shifted the  $V_{\text{dirac}}$  of the GFETs to a positive value, as shown in figure S7(a) [39, 40]. After the ALD process, however, thin (10 nm) yet pinhole-free ALD  $\text{ZrO}_2$  films protected the graphene from the ambient  $\text{H}_2\text{O}$  and  $\text{O}_2$ , leading to a negative shift in  $V_{\text{dirac}}$  (figure 4(c)). With the increasing number of oxygen plasma passes, more continuous films of ALD  $\text{ZrO}_2$  were formed, which passivated graphene from p-doping species and thus induced a further negative shift in  $V_{\text{dirac}}$  of the GFETs (figures S7(b) and S8). Indeed,  $V_{\text{dirac}}$  of ZPG and PZG devices with the ALD  $\text{ZrO}_2$  layer after 30 plasma passes shifted to almost 0 V (figure 4(c)). The passivation effect of ALD  $\text{ZrO}_2$  was also revealed as a dramatic enhancement in the air stability of GFETs. The GFETs showed nearly identical transfer characteristics after exposure to air for 2 weeks (figure S9). Additionally, the ALD  $\text{ZrO}_2$  layer removed charge-carrier trapping sites in graphene, which led to the enhanced drain current of ZPG devices compared to that of PG devices (figures 4(b) and (c)). The increase in drain current of ZPG devices can be also caused by the increase in gate capacitance by deposition of high- $k$  dielectric, e.g.,  $\text{ZrO}_2$ , as a top dielectric layer [41]. However, the increase in gate capacitance should appear as the increase in the slope of GFET transfer curves as well. In our experiment, transfer characteristics of GFETs before and after ALD of  $\text{ZrO}_2$  as a top dielectric did not show much difference in their slope as shown in (figure 4(b)). This indicates that the change in gate capacitance by top dielectric is negligible in this study. Also, we observed the increase in electron mobility and the decrease in hole mobility after ALD of  $\text{ZrO}_2$  on plasma-treated graphene as shown in (figure 4(c)). This asymmetrical change in mobilities is not attributed to a change in gate capacitance that causes symmetrical change in transfer curves of GFETs. Therefore, the increased drain current mainly stems from passivation of charge carrier-trapping sites on graphene by ALD of  $\text{ZrO}_2$  rather than change in gate capacitance. The removal of charge-carrier trapping sites in graphene by ALD of  $\text{ZrO}_2$  also helped the negative shifts in  $V_{\text{dirac}}$  of GFETs because the trap sites are mainly p-doping ones [42].

The dielectric properties of the  $\text{ZrO}_2$  films such as dielectric constant and leakage current density on untreated and

plasma-treated (10 passes) samples were measured using Pt/ $\text{ZrO}_2$ /graphene-structured capacitors. The previous literature on the dielectric property of ALD  $\text{ZrO}_2$  film reported that the dielectric constant of polycrystalline ALD  $\text{ZrO}_2$  film ( $\sim 11$  nm-thick) deposited at high temperature ( $300^\circ\text{C}$ ) is 22–25 [43]. Relatively high dielectric constant ( $\sim 17$ ) of the ALD  $\text{ZrO}_2$  film on plasma-treated (10 passes) graphene indicates that the film is mostly crystallized even at low deposition temperature (figure S10(a)) as was also shown in GIXRD analysis, which is promising for various graphene based electronics and sensors. In contrast, the low dielectric constant ( $\sim 8$ ) of the ALD  $\text{ZrO}_2$  film on untreated graphene confirms the formation of mostly amorphous phase. The leakage current through the  $\text{ZrO}_2$  film on plasma-treated graphene decreased by approximately one order of magnitude compared to that on untreated graphene (figure S10(b)).

The total resistances of the GFETs ( $R_{\text{tot}} = V_{\text{ds}}/I_{\text{d}}$  at the floating gate, where  $V_{\text{ds}}$  is the drain–source voltage and  $I_{\text{d}}$  is the drain current) with various numbers of plasma passes are shown in figure 4(d). The cross-plane resistance of ALD  $\text{ZrO}_2$  is the difference between the total resistances ( $R_{\text{tot}}$ ) of the PZG and ZPG devices. The cross-plane resistance of ALD  $\text{ZrO}_2$  on untreated graphene was virtually zero (figures 4(b) and S11). Because the ALD  $\text{ZrO}_2$  film on untreated graphene had many pinholes (figure 2(a)), source–drain electrodes were in direct contact with the graphene through the pinholes in the  $\text{ZrO}_2$  films, which explains the zero cross-plane resistance. However, as the number of plasma passes increased, the cross-plane resistance and areal coverage of the ALD  $\text{ZrO}_2$  films significantly increased (figures S11 and 2(b)). This suggests that ALD  $\text{ZrO}_2$  films are more densely deposited with increasing numbers of plasma passes, resulting in better passivation effects such as  $V_{\text{dirac}}$  close to zero and good air stability. Also, it is notable that the PG devices with three plasma passes had a lower  $R_{\text{tot}}$  than the PG devices without plasma treatment. This phenomenon is ascribed to the fact that the early stages of oxygen plasma treatment removed organic impurities on graphene that limited the charge transport in graphene [44].

## Conclusion

In conclusion, we have reported the functionalization of multilayer CVD graphene with minimal structural and electrical degradation by atmospheric oxygen plasma treatment. The plasma-treated graphene allowed the growth of thin, polycrystalline, pinhole-free, and relatively uniform ALD  $\text{ZrO}_2$  films on it, even at a low deposition temperature of  $150^\circ\text{C}$ . The facilitated nucleation of ALD  $\text{ZrO}_2$  films on the plasma-treated graphene was due to the formation of O-containing groups such as carbonyl or carboxyl groups, which caused the formation of hydroxyl groups upon exposure to water vapor in air, as proven by XPS analysis. The number of charge-trapping sites decreased by the ALD of  $\text{ZrO}_2$  films on plasma-treated graphene. The ALD  $\text{ZrO}_2$  films worked as an effective passivation layer for graphene, resulting in  $V_{\text{dirac}}$  close to 0 V and the high air stability of

GFETs. Therefore, GFETs with ALD ZrO<sub>2</sub> may find use in flexible electronics and biosensors owing to their low process temperature, high performance, and high stability.

## Acknowledgments

JA acknowledges the financial support from the National Research Foundation under the Ministry of Education, Korea (NRF-2015R1D1A1A01058963), the Ministry of Trade, Industry and Energy (MOTIE), KOREA, through the Education Support program for Creative and Industrial Convergence (Grant Number N0000717), and the Nano-Material Technology Development program through the National Research Foundation of Korea (NRF) funded by the Ministry of Science, ICT and Future Planning (2009-0082580). THL acknowledges support by a Research Grant from Kwangwoon University in 2017 and support by the National Research Foundation of Korea (NRF) grant funded by the Korea government (MSIP) (No. 2016R1C1B1014935). The authors thank Chan Hyung Park for helping with the AFM measurements.

## Conflicts of interest

There are no conflicts to declare.

## ORCID iDs

Tae Hoon Lee  <https://orcid.org/0000-0001-9582-4755>

Jihwan An  <https://orcid.org/0000-0002-7697-9935>

## References

- [1] Kim K S, Zhao Y, Jang H, Lee S Y, Kim J M, Kim K S, Ahn J H, Kim P, Choi J Y and Hong B H 2009 Large-scale pattern growth of graphene films for stretchable transparent electrodes *Nature* **457** 706–10
- [2] Lee S K, Kim B J, Jang H, Yoon S C, Lee C, Hong B H, Rogers J A, Cho J H and Ahn J H 2011 Stretchable graphene transistors with printed dielectrics and gate electrodes *Nano Lett.* **11** 4642–6
- [3] Lee H et al 2016 A graphene-based electrochemical device with thermoresponsive microneedles for diabetes monitoring and therapy *Nat. Nanotechnol.* **11** 566–72
- [4] Lee C, Wei X, Kysar J W and Hone J 2008 Measurement of the elastic properties and intrinsic strength of monolayer graphene *Science* **321** 385–8
- [5] Schwierz F 2010 Graphene transistors *Nat. Nanotechnol.* **5** 487–96
- [6] Shao Y, Wang J, Wu H, Jun L, Aksay I A and Lin Y 2010 Graphene based electrochemical sensors and biosensors: a review *Electroanalysis* **22** 1027–36
- [7] Li N, Zhang X, Song Q, Su R, Zhang Q, Kong T, Liu L, Jin G, Tang M and Cheng G 2011 The promotion of neurite sprouting and outgrowth of mouse hippocampal cells in culture by graphene substrates *Biomaterials* **32** 9374–82
- [8] Yan F, Zhang M and Li J 2014 Solution-gated graphene transistors for chemical and biological sensors *Adv. Healthc. Mater.* **3** 313–31
- [9] Nam H, Oh B, Chen P, Yoon J S, Wi S, Chen M, Kurabayashi K and Liang X 2015 Two different device physics principles for operating MoS<sub>2</sub> transistor biosensors with femtomolar-level detection limits *Appl. Phys. Lett.* **107** 12105
- [10] Lerner M B et al 2014 Scalable production of highly sensitive nanosensors based on graphene functionalized with a designed G protein-coupled receptor *Nano Lett.* **14** 2709–14
- [11] Reddy B et al 2011 High-*k* dielectric Al<sub>2</sub>O<sub>3</sub> nanowire and nanoplate field effect sensors for improved pH sensing *Biomed. Microdevices* **13** 335–44
- [12] Levesque P L, Sabri S S, Aguirre C M, Guillemette J, Siaz M, Desjardins P, Szkopek T and Martel R 2011 Probing charge transfer at surfaces using graphene transistors *Nano Lett.* **11** 132–7
- [13] Ohno Y, Maehashi K, Yamashiro Y and Matsumoto K 2009 Electrolyte-gated graphene field-effect transistors for detecting pH and protein adsorption *Nano Lett.* **9** 3318–22
- [14] Wang X, Tabakman S M and Dai H 2008 Atomic layer deposition of metal oxides on pristine and functionalized graphene *J. Am. Chem. Soc.* **130** 8152–3
- [15] Baitimirova M et al 2016 Tuning of structural and optical properties of graphene/ZnO nanolaminates *J. Phys. Chem. C* **120** 23716–25
- [16] Zaldivar R J, Nokes J P, Adams P M, Hammoud K and Kim H I 2012 Surface functionalization without lattice degradation of highly crystalline nanoscaled carbon materials using a carbon monoxide atmospheric plasma treatment *Carbon* **50** 2966–75
- [17] Shin W C, Bong J H, Choi S Y and Cho B J 2013 Functionalized graphene as an ultrathin seed layer for the atomic layer deposition of conformal high-*k* dielectrics on graphene *ACS Appl. Mater. Interfaces* **5** 11515–9
- [18] Nourbakhsh A et al 2015 Graphene oxide monolayers as atomically thin seeding layers for atomic layer deposition of metal oxides *Nanoscale* **7** 10781–9
- [19] Schutze A, Jeong J Y, Babayan S E, Park J, Selwyn G S and Hicks R F 1998 The atmospheric-pressure plasma jet: a review and comparison to other plasma sources *Plasma Sci. IEEE Trans.* **26** 1685–94
- [20] Li X et al 2009 Large area synthesis of high quality and uniform graphene films on copper foils *Science* **324** 1312–4
- [21] Li X S, Zhu Y W, Cai W W, Borysiak M, Han B Y, Chen D, Piner R D, Colombo L and Ruoff R S 2009 Transfer of large-area graphene films for high-performance transparent conductive electrodes *Nano Lett.* **9** 4359–63
- [22] Eckmann A, Felten A, Mishchenko A, Britnell L, Krupke R, Novoselov K S and Casiraghi C 2012 Probing the nature of defects in graphene by Raman spectroscopy *Nano Lett.* **12** 3925–30
- [23] Xiao N et al 2011 Enhanced thermopower of graphene films with oxygen plasma treatment *ACS Nano* **5** 2749–55
- [24] Elias D C et al 2009 Control of graphene's properties by reversible hydrogenation: evidence for graphane *Science* **323** 610–3
- [25] McEvoy N, Nolan H, Ashok Kumar N, Hallam T and Duesberg G S 2013 Functionalisation of graphene surfaces with downstream plasma treatments *Carbon* **54** 283–90
- [26] Zhou P, Yang S, Sun Q, Chen L, Wang P, Ding S and Zhang D W 2014 Direct deposition of uniform high- $\kappa$  dielectrics on graphene *Sci. Rep.* **4** 6448
- [27] Hausmann D M, Kim E, Becker J and Gordon R G 2002 Atomic layer deposition of hafnium and zirconium oxides using metal amide precursors *Chem. Mater.* **14** 4350–8

- [28] Chang J P and Lin Y S 2001 Dielectric property and conduction mechanism of ultrathin zirconium oxide films *Appl. Phys. Lett.* **79** 3666–8
- [29] Kukli K, Ritala M, Aarik J, Uustare T and Leskelä M 2005 Influence of growth temperature on properties of zirconium dioxide films grown by atomic layer deposition *J. Appl. Phys.* **92** 1833–40
- [30] Liu J, Meng X, Hu Y, Geng D, Banis M N, Cai M, Li R and Sun X 2013 Controlled synthesis of zirconium oxide on graphene nanosheets by atomic layer deposition and its growth mechanism *Carbon* **52** 74–82
- [31] Hausmann D M and Gordon R G 2003 Surface morphology and crystallinity control in the atomic layer deposition (ALD) of hafnium and zirconium oxide thin films *J. Cryst. Growth* **249** 251–61
- [32] Aarik J, Aidla A, Uustare T and Sammelselg V 1995 Morphology and structure of TiO<sub>2</sub> thin films grown by atomic layer deposition *J. Cryst. Growth* **148** 268–75
- [33] Jariwala D, Marks T J and Hersam M C 2016 Mixed-dimensional van der Waals heterostructures *Nat. Mater.* **16** 170–81
- [34] Vanderbilt D, Zhao X and Ceresoli D 2005 Structural and dielectric properties of crystalline and amorphous ZrO<sub>2</sub> *Thin Solid Films* **486** 125–8
- [35] Lafkioti M, Krauss B, Lohmann T, Zschieschang U, Klauk H, Klitzing K V and Smet J H 2010 Graphene on a hydrophobic substrate: doping reduction and hysteresis suppression under ambient conditions *Nano Lett.* **10** 1149–53
- [36] Nourbakhsh A, Cantoro M, Klekachev A V, Pourtois G, Vosch T, Hofkens J, Van Der Veen M H, Heyns M M, De Gendt S and Sels B F 2011 Single layer vs bilayer graphene: a comparative study of the effects of oxygen plasma treatment on their electronic and optical properties *J. Phys. Chem. C* **115** 16619–24
- [37] Pirkle A, Chan J, Venugopal A, Hinojos D, Magnuson C W, McDonnell S, Colombo L, Vogel E M, Ruoff R S and Wallace R M 2011 The effect of chemical residues on the physical and electrical properties of chemical vapor deposited graphene transferred to SiO<sub>2</sub> *Appl. Phys. Lett.* **99** 122108
- [38] Giovannetti G, Khomyakov P A, Brocks G, Karpan V M, van Den Brink J and Kelly P J 2008 Doping graphene with metal contacts *Phys. Rev. Lett.* **101** 26803
- [39] Kim K, Park H J, Woo B C, Kim K J, Kim G T and Yun W S 2008 Electric property evolution of structurally defected multilayer graphene *Nano Lett.* **8** 3092–6
- [40] Nourbakhsh A, Cantoro M, Vosch T, Pourtois G, Clemente F, van der Veen M H, Hofkens J, Heyns M M, De Gendt S and Sels B F 2010 Bandgap opening in oxygen plasma-treated graphene *Nanotechnology* **21** 435203
- [41] Xia J L, Chen F, Wiktor P, Ferry D K and Tao N J 2010 Effect of top dielectric medium on gate capacitance of graphene field effect transistors: implications in mobility measurements and sensor applications *Nano Lett.* **10** 5060–4
- [42] Kang C G, Lee Y G, Lee S K, Park E, Cho C, Lim S K, Hwang H J and Lee B H 2013 Mechanism of the effects of low temperature Al<sub>2</sub>O<sub>3</sub> passivation on graphene field effect transistors *Carbon* **53** 182–7
- [43] Lee S Y, Kim H, McIntyre P C, Saraswat K C and Byun J S 2003 Atomic layer deposition of ZrO<sub>2</sub> on W for metal-insulator-metal capacitor application *Appl. Phys. Lett.* **82** 2874–6
- [44] Peltekis N, Kumar S, McEvoy N, Lee K, Weidlich A and Duesberg G S 2012 The effect of downstream plasma treatments on graphene surfaces *Carbon* **50** 395–403